Eur. Phys. J. C (2016) 76:573
DOI 10.1140/epjc/s10052-016-4427-8

THE EUROPEAN PHYSICAL JOURNAL C

Regular Article - Theoretical Physics

$Z_c(3900)$: confronting theory and lattice simulations

Miguel Albaladejo[a], **Pedro Fernandez-Soler, Juan Nieves**

Instituto de Física Corpuscular (IFIC), Centro Mixto CSIC-Universidad de Valencia, Institutos de Investigación de Paterna, Aptdo. 22085, 46071 Valencia, Spain

Received: 10 June 2016 / Accepted: 10 October 2016 / Published online: 24 October 2016

Abstract We consider a recent T-matrix analysis by Albaladejo et al. (Phys Lett B 755:337, 2016), which accounts for the $J/\psi\pi$ and $D^*\bar{D}$ coupled-channels dynamics, and which successfully describes the experimental information concerning the recently discovered $Z_c(3900)^{\pm}$. Within such scheme, the data can be similarly well described in two different scenarios, where $Z_c(3900)$ is either a resonance or a virtual state. To shed light into the nature of this state, we apply this formalism in a finite box with the aim of comparing with recent Lattice QCD (LQCD) simulations. We see that the energy levels obtained for both scenarios agree well with those obtained in the single-volume LQCD simulation reported in Prelovsek et al. (Phys Rev D 91:014504, 2015), thus making it difficult to disentangle the two possibilities. We also study the volume dependence of the energy levels obtained with our formalism and suggest that LQCD simulations performed at several volumes could help in discerning the actual nature of the intriguing $Z_c(3900)$ state.

1 Introduction

Since the discovery of the $X(3872)$ in 2003 [1], the charmonium and charmonium-like spectrum are continuously being enlarged with new so-called XYZ states [2–4], many of which do not fit properly in the conventional quark models [5]. The relevance of meson–meson channels can be grasped from the fact that all the charmonium states predicted below the lowest hidden-charm threshold ($D\bar{D}$) have been experimentally confirmed, but above this energy most of the observed states cannot be unambiguously identified with any of the predicted charmonium $c\bar{c}$ states.

Among the XYZ states, $Z_c(3900)^{\pm}$ was simultaneously discovered by the BESIII and Belle collaborations [6,7] in the $e^+e^- \to Y(4260) \to J/\psi\pi^+\pi^-$ reaction, where a clear peak very close to the $D^*\bar{D}$ threshold, around 3.9 GeV, is seen in the $J/\psi\pi$ spectrum. Later on, an analysis [8] based on CLEO-c data for a different reaction, $e^+e^- \to \psi(4160) \to J/\psi\pi^+\pi^-$, confirmed the presence of this resonant structure as well, although with a somewhat lower mass. The BESIII collaboration [9,10] has also reported a resonant-like structure in the $\bar{D}^*D$ spectrum for the reaction $e^+e^- \to \bar{D}^*D\pi$ at different e^+e^- center-of-mass (c.m.) energies [including the production of $Y(4260)$]. This structure, with favored quantum numbers $J^P = 1^+$, has been cautiously called $Z_c(3885)^{\pm}$, because its fitted mass and width showed some differences with those attributed to $Z_c(3900)^{\pm}$. Whether both sets of observations correspond to the same state needs to be confirmed, though there is a certain consensus that this is indeed the case, and the peaks reported as $Z_c(3885)^{\pm}$ and $Z_c(3900)^{\pm}$ originate from the same state seen in different channels. Moreover, evidence for its neutral partner, $Z_c(3900)^0$, has also been reported [8,11].

The nature of $Z_c(3900)^{\pm}$ is intriguing. On one hand, it couples to $D^*\bar{D}$ and $J/\psi\pi$, and therefore one assumes it should contain a constituent $c\bar{c}$ quark–anti-quark pair. On the other hand, it is charged and hence it must also have another constituent quark–anti-quark pair, namely $u\bar{d}$ (for Z_c^+). Its minimal structure would then be $c\bar{c}u\bar{d}$, which automatically qualifies it as a non-$q\bar{q}$ (exotic) meson. Being a candidate for an exotic hidden-charm state, it has triggered much theoretical interest. An early discussion of possible structures for $Z_c(3900)^{\pm}$ was given in Ref. [12]. The suggested interpretations cover a wide range: a $\bar{D}^*D$ molecule [13–20], a tetraquark [21–27], an object originating from an attractive $\bar{D}^*D^*$ interaction [28], a simple kinematical effect [29,30], a cusp enhancement due to a triangle singularity [31], or a radially excited axial meson [32]. In Ref. [33], it was argued that this structure cannot be a kinematical effect and that it must necessarily originate from a nearby pole. Consequences from some of these models have been discussed in Ref. [34]. The non-compatibility (partial or total) of the properties of Z_c

[a] e-mail: miguelalbaladejo@gmail.com

deduced in different approaches clearly hints why the actual nature of this state has attracted so much attention.

In Ref. [35], which is the theoretical basis of the present manuscript, a $J/\psi\pi$–$D^*\bar{D}$ coupled-channel scheme was proposed to describe the observed peaks associated to the $Z_c(3900)$, which is assumed to have $I(J^{PC}) = 1(1^{+-})$ quantum numbers.[1] Within this coupled-channel scheme, it was possible to successfully describe simultaneously the BESIII $J\psi\pi$ [6] and $D^*\bar{D}$ [10] invariant mass spectra, in which the $Z_c(3900)^{\pm}$ structure has been seen. Interestingly, two different fits with similar quality were able to reproduce the data. In each of them, the origin of the $Z_c(3900)^{\pm}$ was different. In the first scenario, it corresponded to a resonance originating from a pole above the $D^*\bar{D}$ threshold, whereas in the second one the structure was produced by a virtual pole below the threshold (see Ref. [35] for more details).

Hadron interactions are governed by the non-perturbative regime of QCD and, for this reason, Lattice QCD (LQCD) is an essential theoretical tool in hadron physics. In particular, one of the aims of LQCD is to obtain the hadron spectrum from quarks and gluons and their interactions (see e.g. Ref. [36] for a review focused on the light sector, and Refs. [37–40] for results concerning the charmonium sector). For such a purpose the Lüscher method [41,42] is widely used. It relates the discrete energy levels of a two-hadron system in a finite box with the phase shifts and/or binding energies of that system in an infinite volume. Appropriate generalizations relevant for our work can be found in Refs. [43–46].

LQCD simulations devoted to finding the $Z_c(3900)$ state are still scarce [47–52]. Exploratory theoretical studies for hidden-charm molecules have been performed in Refs. [53,54], while actual LQCD simulations [47–51] find energy levels showing a weak interaction in the $Z_c(3900)^{\pm}$ quantum numbers sector (either attractive or repulsive), and no evidence is found for its existence. The work of Ref. [52] employs LQCD to obtain a coupled-channel S-matrix, which shows an interaction dominated by off-diagonal terms, and, according to Ref. [52], this does not support the usual resonance picture for $Z_c(3900)$. This S-matrix contains a pole located well below threshold in an unphysical Riemann sheet, i.e., a virtual pole. It is worth to note that this possibility could be in agreement with the second scenario advocated in Ref. [35], and mentioned above.

Our objective in the present manuscript is to implement the coupled-channel T-matrix fitted to data in Ref. [35] in a finite volume and study its spectrum. Thus, we will be able to compare the energy levels obtained with this finite volume T-matrix with those obtained in LQCD simulations, in particular those reported in Ref. [48]. This work is organized as follows. The formalism is presented in Sect. 2, while the T-matrix of Ref. [35] is briefly discussed in Sect. 2.1, and its extension for a finite volume is outlined in Sect. 2.2. Results are presented and discussed in Sect. 3, and the conclusions of this work, together with a brief summary are given in Sect. 4.

[1] Through all this work, charge conjugation refers only to the neutral element of the $Z_c(3900)$ isotriplet.

2 Formalism

2.1 Infinite volume

We first briefly review the model of Ref. [35] (where the reader is referred for more details) that we are going to employ here. There, the $Y(4260)$ decays to $D\bar{D}^*\pi$ and $J/\psi\pi\pi$ are studied with a model shown diagrammatically in Fig. 1 of that reference. Final state interactions among the outgoing $D\bar{D}^*$ and $J/\psi\pi$ produce the peaks observed by the BESIII collaboration, which are associated to the $Z_c(3900)$ state. The two channels involved in the $1(1^+)$ T-matrix are denoted as $1 \equiv J/\psi\pi$ and $2 \equiv D\bar{D}^*$. Solving the on-shell version of the factorized Bethe–Salpeter equation (BSE) allows one to write:

$$T^{-1}(E) = V^{-1}(E) - G(E), \tag{1}$$

where E is the c.m. energy of the system. The symmetric V matrix is the potential kernel, and its matrix elements have the following form:

$$V_{ij} = 4\sqrt{m_{i,1}m_{i,2}m_{j,1}m_{j,2}}\, C_{ij}\, e^{-k_i^2/\Lambda_i^2} e^{-k_j^2/\Lambda_j^2}, \tag{2}$$

with $m_{i,1}$ and $m_{i,2}$ the masses of the particles of the ith channel and k_i^2, the relative three-momenta squared in the c.m. frame, implicitly defined through:

$$E = \omega_\psi(k_1) + \omega_\pi(k_1), \tag{3}$$

$$E = \omega_{D^*\bar{D}}(k_2)\,, \tag{4}$$

where

$$\omega_\psi(q) = \sqrt{m_{J/\psi}^2 + q^2}\,, \tag{5}$$

$$\omega_\pi(q) = \sqrt{m_\pi^2 + q^2}\,, \tag{6}$$

$$\omega_{D^*\bar{D}}(q) = m_D + m_{D^*} + \frac{m_D + m_{D^*}}{2m_D m_{D^*}} q^2\,, \tag{7}$$

with $q \equiv |\vec{q}\,|$. The Gaussian form factors $e^{-k_i^2/\Lambda_i^2}$ are introduced to regularize the BSE, and thus, for each channel, an ultraviolet (UV) cut-off Λ_i is introduced. In this work, we have used $\Lambda_1 = 1.5$ GeV and two values for $\Lambda_2 = 0.5$ and 1 GeV [55,56]. The C_{ij} matrix stands for the S-wave interaction in the coupled-channel space, and it is given by [35]:

Table 1 Values of the parameters employed in Eq. (8), taken from Ref. [35], together with the Z_c pole positions found in that work. The errors account for statistical (first) and systematic (second) uncertainties (see Ref. [35] for details)

Λ_2 (GeV)	C_{1Z} (fm^2)	b (fm^3)	$\widetilde{C}$ (fm^2)	M_{Z_c} (MeV)	$\Gamma_{Z_c}/2$ (MeV)
1.0	$-0.19 \pm 0.08 \pm 0.01$	$-2.0 \pm 0.7 \pm 0.4$	$0.39 \pm 0.10 \pm 0.02$	$3894 \pm 6 \pm 1$	$30 \pm 12 \pm 6$
0.5	$0.01 \pm 0.21 \pm 0.03$	$-7.0 \pm 0.4 \pm 1.4$	$0.64 \pm 0.16 \pm 0.02$	$3886 \pm 4 \pm 1$	$22 \pm 6 \pm 4$
1.0	$-0.27 \pm 0.08 \pm 0.07$	0 (fixed)	$0.34 \pm 0.14 \pm 0.01$	$3831 \pm 26^{+7}_{-28}$	Virtual state
0.5	$-0.27 \pm 0.16 \pm 0.13$	0 (fixed)	$0.54 \pm 0.16 \pm 0.02$	$3844 \pm 19^{+12}_{-21}$	Virtual state

$$C = \begin{bmatrix} 0 & \tilde{C} \\ \tilde{C} & C_{22}(E) \end{bmatrix}. \tag{8}$$

In Eq. (8) the $J/\psi\pi \to J/\psi\pi$ interaction is neglected, $C_{11} = 0$, the inelastic transition one is approximated by a constant, $\tilde{C}$, while the $D^*\bar{D} \to D^*\bar{D}$ potential $C_{22}(E)$ is parametrized as:

$$C_{22}(E) = C_{1Z} + b\,(E - m_D - m_{D^*})\,. \tag{9}$$

In a momentum expansion, the lowest order contact potential for this elastic transition would be simply a constant, $C_{22} \equiv C_{1Z}$. However, it is easy to prove that two coupled channels with contact potentials cannot generate a resonance above threshold. Thus and for the sake of generality, the model of Ref. [35] allows for an energy dependence in Eq. (9), driven by the b parameter. The G matrix in Eq. (1) is diagonal, and its matrix elements are the $J/\psi\pi$ and $D^*\bar{D}$ loop functions,

$$G_{11}(E) = \int_{\mathbb{R}^3} \frac{\mathrm{d}^3 q}{(2\pi)^3} \frac{\omega_\psi(q) + \omega_\pi(q)}{2\omega_\psi(q)\omega_\pi(q)} \times \frac{e^{-2(q^2-k_1^2)/\Lambda_1^2}}{E^2 - \left(\omega_\psi(q) + \omega_\pi(q)\right)^2 + i\epsilon}\,, \tag{10}$$

$$G_{22}(E) = \frac{1}{4 m_D m_{D^*}} \int_{\mathbb{R}^3} \frac{\mathrm{d}^3 q}{(2\pi)^3} \frac{e^{-2(q^2-k_2^2)/\Lambda_2^2}}{E - \omega_{D\bar{D}^*}(q) + i\epsilon}\,, \tag{11}$$

which account for the right-hand cut of the T-matrix, which satisfies in this way the optical theorem. The $D^*\bar{D}$ channel loop function G_{22} is computed in the non-relativistic approximation.

Resonances, bound states or virtual states are found as poles in one or more of the different Riemann sheets of the amplitude, which are reached by analytical continuation of the loop functions (Eqs. (10) and (11)) that enter in the evaluation of the T-matrix (Eq. (1)). The different Riemann sheets, each one denoted $(\eta_1\eta_2)$, are defined by the following continuations:

$$G_{11}(E) \to G_{11}(E) + \eta_1 i \frac{k_1(E)}{4\pi E}\,, \tag{12}$$

$$G_{22}(E) \to G_{22}(E) + \eta_2 i \frac{k_2(E)}{4\pi (m_D + m_{D^*})}\,, \tag{13}$$

where $\eta_{1,2}$ take the values 0 or 1. The physical Riemann sheet is thus denoted by (00).

The free parameters in the interaction matrix C ($\tilde{C}$, C_{1Z} and b) were fitted in Ref. [35] to the experimental $J/\psi\pi^-$ and D^+D^{*-} invariant mass distributions in the $Y(4260) \to J/\psi\pi\pi$ and $Y(4260) \to D\bar{D}^*\pi$ decays [6,10]. The fitted parameters are compiled here in Table 1, where we can see the two different scenarios investigated in Ref. [35]. In the first one, $b \neq 0$, Z_c appears as a $D^*\bar{D}$ resonance, i.e., a pole above the $D^*\bar{D}$ threshold in the (11) Riemann sheet, connected with the physical one above this threshold. In the second one, where $b = 0$, a pole appeared below the $D\bar{D}^*$ threshold in the (01) Riemann sheet, which gives rise to the $Z_c(3900)$ structure, peaking exactly at the $D^*\bar{D}$ threshold in this case [35]. As mentioned above, the pole is placed below the $D\bar{D}^*$ threshold, but it is above the $J/\psi\pi$ one, so it has a small imaginary part (about 8 MeV). We still regard it as a virtual pole, since, if the $J/\psi\pi$ channel is switched off (by setting the $D\bar{D}^* \to J/\psi\pi$ transition potential to zero, $\tilde{C} = 0$), it moves to the real axis in the unphysical Riemann sheet of the $D\bar{D}^*$ elastic amplitude, T_{22} (see also Ref. [57]). In both scenarios, $b \neq 0$ and $b = 0$, only one pair of complex-conjugate poles appears, and it does appear in only one Riemann sheet.

2.2 Finite volume

LQCD simulations are carried out in a finite volume cubic lattice. Since rotational symmetry is broken in the box, partial waves can mix in general. We are concerned in this work with the S-wave ($\ell = 0$) amplitude, for which the lowest partial wave it could mix with is the G-wave ($\ell = 4$), since we are considering pseudoscalar–vector scattering with zero total momentum. (Non-zero total momentum could lead to mixing with other, lower waves.) The G-wave is high enough so that its effect is expected to be small, and hence we neglect it in this work. (For further discussion about this issue in a context similar to that of this work, see e.g. Refs. [46,58].)

In this section, the coupled-channel T-matrix explained in Sect. 2.1 is studied in a finite volume. The consequence of putting the interaction in a box of size L with periodic boundary conditions is that the three-momentum is no longer

a continuous variable, but a discrete one. For each value of L, we have the infinite set of momenta $\vec{q} = \frac{2\pi}{L}\vec{n}$, $\vec{n} \in \mathbb{Z}^3$. The integrals in Eqs. (10) and (11) will be replaced by sums over all the possible values of $\vec{q}$:

$$\tilde{G}_{11}(E) = \frac{1}{L^3}\sum_{\vec{n}} \frac{\omega_\psi(q)+\omega_\pi(q)}{2\omega_\psi(q)\omega_\pi(q)} \frac{e^{-2(q^2-k_1^2)/\Lambda_1^2}}{E^2-\left(\omega_\psi(q)+\omega_\pi(q)\right)^2}\,, \tag{14}$$

$$\tilde{G}_{22}(E) = \frac{1}{4\,(m_D m_{D^*})}\frac{1}{L^3}\sum_{\vec{n}} \frac{e^{-2(q^2-k_2^2)/\Lambda_2^2}}{E-\omega_{D\bar{D}^*}(q)} \tag{15}$$

(see Ref. [53] for further details). The T-matrix in a finite volume is then:

$$\tilde{T}^{-1}(E) = V^{-1}(E) - \tilde{G}(E)\,, \tag{16}$$

where the $\tilde{G}$ matrix elements are given by Eqs. (14) and (15). The discrete energy levels in the finite box are given by the poles of the $\tilde{T}$-matrix. If the interaction is switched off, $V \to 0$, the free (or non-interacting) energy levels are given by the poles of the $\tilde{G}_{ii}$ functions,

$$E^{(\vec{n}^{\,2})}_{J/\psi\pi} = \omega_\psi(q_L n) + \omega_\pi(q_L n)\,, \tag{17}$$

$$E^{(\vec{n}^{\,2})}_{D^*\bar{D}} = \omega_{D\bar{D}^*}(q_L n)\,, \tag{18}$$

where we use the shorthand $q_L = 2\pi/L$, and $n = \sqrt{\vec{n}^{\,2}}$. The effect of the interaction is to shift these non-interacting energy levels.

Our purpose is to make contact with the results reported in the LQCD simulation of Ref. [48], and hence we will employ the masses and the energy-momentum dispersion relations used in that work. For the $J/\psi\pi$ channel the dispersion relation in Eq. (3) is still appropriate, but for the case of the $D^*\bar{D}$ channel, in Eqs. (4) and (7), $\omega_{D\bar{D}^*}(q)$ must be replaced by [48,59]:

$$\omega^{\rm lat}_{D\bar{D}^*}(q) = m_{D,1} + m_{D^*,1} + \frac{m_{D,2}+m_{D^*,2}}{2m_{D,2}m_{D^*,2}}q^2 - \frac{m^3_{D,4}+m^3_{D^*,4}}{8m^3_{D,4}m^3_{D^*,4}}q^4\,. \tag{19}$$

This lattice energy of the $D^*\bar{D}$ pair suffers from discretization errors and it must be used in Eq. (15). The non-interacting energy levels in Eq. (18) should also be modified accordingly. Notice that, because of the factor e^{-q^2/Λ^2}, the sum in Eq. (15) is exponentially suppressed in $\vec{n}^{\,2}$. For the range of energies considered in this work, it is sufficient to add terms up to $\vec{n}^{\,2} = 6$.[2] Finally, the discrete, interacting energy levels

[2] We have checked that the numerical differences are negligible if larger values, say $\vec{n}^{\,2} = 8$, are used.

Table 2 Lattice parameters taken from Refs. [48,59], and employed in this work

Lengths (fm)	
a	0.1239 (13)
$L = 16a$	1.982 (21)
Masses (lattice units)	
am_π	0.1673 (16)
$am_{J/\psi}$	1.54171 (43)
am_{η_c}	1.47392 (31)
$am_{D,1}$	0.9801 (10)
$am_{D,2}$	1.107 (12)
$am_{D,4}$	1.107 (27)
$am_{D^*,1}$	1.0629 (13)
$am_{D^*,2}$	1.267 (21)
$am_{D^*,4}$	1.325 (68)

reported in Ref. [48] are actually the result of applying the following shift:

$$E \to E^* = E - m^{\rm lat}_{\rm s.a.} + m^{\rm exp}_{\rm s.a.}\,, \tag{20}$$

where the spin-average mass $m_{\rm s.a.}$ is given by $m_{\rm s.a.} = \frac{1}{4}(m_{\eta_c} + 3m_{J/\psi})$. For this reason, we will also present our energy levels shifted as in Eq. (20). The parameters involved in our calculations, taken from Refs. [48,59], are collected in Table 2. In particular, one has $m_\pi = 266 \pm 4$ MeV and $L = 16\,a = 1.98 \pm 0.02$ fm, where a is the lattice spacing.

2.3 Further comments

With all the ingredients presented in Sect. 2.2, we can compare our predictions for the energy levels in a box with those reported in Ref. [48]. But before presenting our results we would like to discuss some technical details concerning two differences that could affect the comparison.

First, we would like to note that the LQCD simulation in Ref. [48] includes the $J/\psi\pi$ and $D^*\bar{D}$ channels that are present in our T-matrix analysis, but it also includes other channels, like $\eta_c\rho$ or $D^*\bar{D}^*$, the thresholds of which are located 120 MeV below and 140 MeV above the $D\bar{D}^*$ threshold, respectively. However, according to Ref. [35], it is sufficient to include the $J/\psi\pi$ and $D^*\bar{D}$ channels to achieve a good reproduction of the experimental information concerning $Z_c(3900)$. For this reason, we expect that, in first approximation, these other channels could be safely neglected in the calculations. It must be stated that there are also three-meson channels with thresholds below the $D^*\bar{D}$ one, like $\eta_c\pi\pi$ ($\sim$ 3260 MeV) or $J/\psi\pi\pi$ ($\sim$ 3370 MeV) among others, and also above the $D^*\bar{D}$ threshold, such as $D^*\bar{D}\pi$ ($\sim$4015 MeV), which could give rise to energy levels in the

region we are exploring. These channels are neither explicitly taken into account in Ref. [48] nor in the present approach.

Next, we would like to briefly mention the m_π dependence of our predictions and of LQCD simulations. In general, the properties of resonances vary, to a larger or lesser extent, with the quark masses. LQCD simulations are usually performed with quark masses different from the physical ones, and hence the resonance parameters extracted from them can also be different from the experimental ones.[3] From a theoretical point of view, the pion mass dependence (in general, the quark mass dependence) will manifest itself both in the kinematics of the processes and in the dynamics of the interactions. In our particular case, there could be a pion mass dependence in the parameters of the potential, Eq. (8). Nonetheless, the LQCD simulation of Ref. [48] is performed for a relatively low pion mass, $m_\pi = 266 \pm 4$ MeV, and we thus expect the eventual dependence to be mild, so we have ignored it. Furthermore, we are going to compare several sets of these parameters (presented in Table 1), which somewhat compensates this effect.

3 Results and discussion

In Fig. 1, we show the L dependence of some energy levels close to the $D^*\bar{D}$ threshold. They have been computed from the poles of the finite volume $\tilde{T}$-matrix, Eq. (16), by using the parameters of Table 1 for $\Lambda_2 = 1$ GeV, and the lattice setup given in Table 2. The levels obtained in the $Z_c(3900)^\pm$ resonance (virtual) scenario, calculated using the entries of the first (third) row of Table 1, are displayed in the left (right) panel. The blue dashed lines stand for the $J/\psi\pi$–$D^*\bar{D}$ coupled-channel-analysis results, and the red solid lines show the energy levels obtained when the inelastic $J/\psi\pi$–$D^*\bar{D}$ transition is neglected ($\tilde{C} = 0$). This latter case corresponds to considering a single, elastic channel ($D^*\bar{D}$). The error bands account for the uncertainties on the energy levels inherited from the errors in the parameters of Ref. [35], quoted in Table 1 (statistical and systematical errors are added in quadrature for the calculations). The green dashed (dotted-dashed) lines stand for the non-interacting $D^*\bar{D}$ ($J/\psi\pi$) energy levels. In Fig. 2, the same results are shown but for the case $\Lambda_2 = 0.5$ GeV. The qualitative L behavior of both Figs. 1 and 2 is similar, so we discuss first Fig. 1 and, later on, the specific differences between them will be outlined.

For both resonant and virtual scenarios, there is always an energy level very close to a free energy of the $J/\psi\pi$ state, $E^{(l)}_{J/\psi\pi}$, which reveals that the interaction driven by this meson pair is weak. Furthermore, the energy levels for the coupled-channel $\tilde{T}$-matrix basically follow those obtained within the elastic $D^*\bar{D}$ approximation, except in the neighborhood of the $J/\psi\pi$ free energies. This also corroborates that the role of the $J/\psi\pi$ is not essential.

Let us pay attention to the levels placed in the vicinity of the $D^*\bar{D}$ threshold. For simplicity, we first look at the single elastic channel case. There appears always a state just below threshold, as it should occur since we are putting an attractive interaction in a finite box. As the size of the box increases, and since there is no bound state in the infinite volume limit (physical case), this level approaches the threshold.[4] When the $J/\psi\pi$ channel is switched on, the $L-$behavior of this level will be modified, specially when it is close to a discrete $J/\psi\pi$ free energy. Note that the slopes of the $J/\psi\pi$ free levels, in the range of energies considered here, are larger (in absolute value) than those of the $D\bar{D}^*$ ones, because the threshold of the $J/\psi\pi$ channel is far from the region studied.

From the above discussion, one realizes that the next coupled-channel energy level, located between the two $D^*\bar{D}$ free ones ($E^{(0)}_{D^*\bar{D}}$ and $E^{(1)}_{D^*\bar{D}}$), could be more convenient to extract details of the $Z_c(3900)^\pm$ dynamics. Indeed, in the resonance scenario, this second energy level is very shifted downwards with respect to $E^{(1)}_{D^*\bar{D}}$, since it is attracted towards the Z_c resonance energy.[5] In this context, it should be noted that the presence of $Z_c(3900)^\pm$ does not induce the appearance of an additional energy level, but a sizable shift of the energy levels with respect to the non-interacting ones. Therefore, even if no extra energy level appears, it would not be possible to completely discard the existence of a physical state (resonance). The energy shift, however, can be quite large and, only in this sense, one might speak of the appearance of an additional energy level. The correction of the second energy level in the virtual state scenario is much less pronounced. We should note here that the elastic phase shift computed with the T-matrix in Ref. [35] does not follow the

[3] As an example, let us consider the recent work of Refs. [60,61], where LQCD simulations concerning the light sector are performed for pion and kaon masses $m_\pi = 391$ MeV and $m_K = 549$ MeV. Although the spectrum found there cannot easily be compared with the physical (experimental) one because of the large masses used, qualitative comparisons can still be made, which are in good agreement with the observed spectrum or with theoretical expectations. In particular, in Ref. [61] the $\eta\pi$, $K\bar{K}$ interaction is studied and a cusp behavior in the $\eta\pi$ elastic amplitude is traced back to the $a_0(980)$ resonance. In Ref. [60], where the ηK, πK interactions are considered, resonances are found alongside with a virtual state and a bound state. The virtual state in the sector $J^P = 0^+$ is expected to evolve to a resonance with decreasing quark masses, and may thus be identified with the κ resonance. This is in agreement with the theoretically expected behavior for the κ resonance [62], and also for the σ [63,64], the $I = 0$ member of the octet.

[4] This is also discussed, in more detail, in Ref. [53].

[5] For physical pions ($m_\pi \sim 140$ MeV), the Z_c resonance mass, ignoring errors, is 3894 MeV (3886 MeV) for $\Lambda_2 = 1$ GeV (0.5 GeV), as seen from Table 1. For $m_\pi = 266$ MeV as used in Ref. [48], and taking into account the shift in Eq. (20), one might estimate that mass to be around 3912 MeV (3902 MeV).

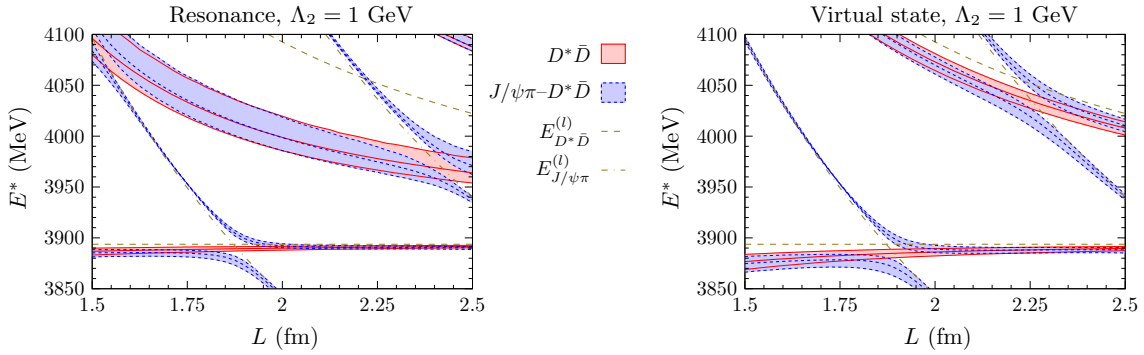

Fig. 1 Volume dependence of some energy levels located close to the $D^*\bar{D}$ threshold, and obtained when Z_c is described as a resonance (*left*) or as a virtual state (*right*) in the $L \to \infty$ limit. The *blue dashed lines* have been obtained from the $J/\psi\pi$–$D^*\bar{D}$ coupled-channel analysis, and the *red solid lines* show the single elastic channel ($D^*\bar{D}$) case, in both cases Λ_2 has been fixed to 1 GeV. The error bands are obtained from the uncertainties of the parameters introduced in the theoretical model of Ref. [35] (Table 1), adding in quadratures the statistical and systematic errors. The *green dashed* (*dotted-dashed*) *lines* are the free $D^*\bar{D}$ ($J/\psi\pi$) energy levels $E^{(l)}_{D^*\bar{D}}$ ($E^{(l)}_{J/\psi\pi}$)

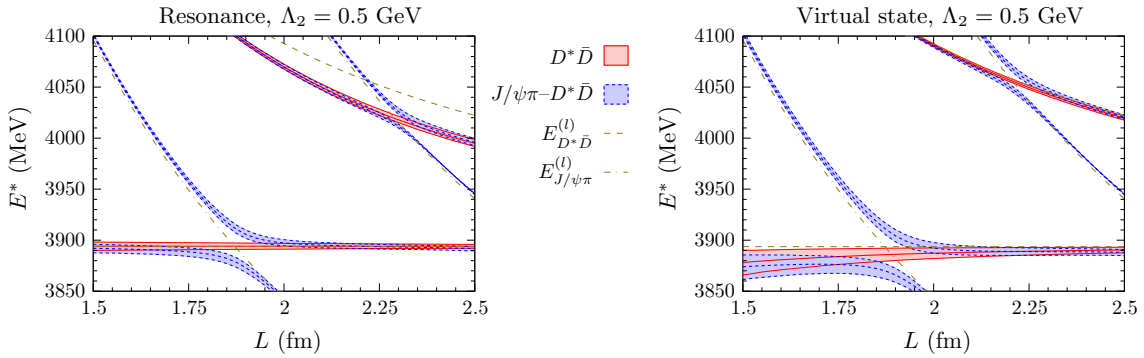

Fig. 2 Same as in Fig. 1, but for the case $\Lambda_2 = 0.5$ GeV

pattern of a standard Breit–Wigner distribution associated with a narrow resonance. Indeed, the phase shift does not change quickly from 0 to π in the vicinity of the $Z_c(3900)$ mass, and actually it does not even reach $\pi/2$. This is mostly due to a sizable background in the amplitude.

We now compare the cases $\Lambda_2 = 1$ GeV (Fig. 1) and $\Lambda_2 = 0.5$ GeV (Fig. 2). For $\Lambda_2 = 0.5$ GeV, the relevant (second) energy level is more shifted with respect to $E^{(1)}_{D^*\bar{D}}$ in the resonance scenario (Fig. 2, left) than in the virtual scenario (Fig. 2, right). This is the same behavior already discussed for $\Lambda_2 = 1$ GeV. However, the shift for the resonance scenario is smaller in the $\Lambda_2 = 0.5$ GeV case (Fig. 2, left) than in the $\Lambda_2 = 1$ GeV one (Fig. 1, left). This is due to the fact that $Z_c(3900)^{\pm}$ is closer to the threshold and the coupling to $D^*\bar{D}$ is smaller for the $\Lambda_2 = 0.5$ GeV case. Another important difference between the $\Lambda_2 = 1$ GeV and $\Lambda_2 = 0.5$ GeV results is that the error band of the relevant energy level is smaller when the lighter cut-off is used. This is due to the different relative errors in both cases, and the fact that, for $\Lambda_2 = 0.5$ GeV, the relevant level is closer to the $E^{(1)}_{D^*\bar{D}}$ free energy than in the $\Lambda_2 = 1$ GeV case.

After having explored the volume dependence of the energy levels predicted with our $\tilde{T}$-matrix and scrutinized its physical meaning, we can now compare our results with those reported in Ref. [48]. The energy levels in the latter work are obtained from a single-volume simulation, $L = 1.98 \pm 0.02$ fm, and are shown in Fig. 3 with black squares. In the figure, we also show the results obtained in this work for $L = 2$ fm, for both the resonance (filled circles) and the virtual state (empty circles) scenarios for the $Z_c(3900)$. Besides, the energy levels calculated with $\Lambda_2 = 1$ GeV and $\Lambda_2 = 0.5$ GeV are represented in blue and green, respectively. We provide two different error bars for our results, considering only the uncertainties of the parameters entering in the T-matrix (Table 1), or additionally taking into account the errors of the lattice parameters (Table 2). We clearly see three distinct regions, the lowest energies are very close to the $D\bar{D}^*$ threshold ($E^{(0)}_{D^*\bar{D}}$) and to the first $J/\psi\pi$ free energy level ($E^{(1)}_{J/\psi\pi}$). These free energies are shown in Fig. 3 with red solid horizontal lines. As expected, the two lowest lattice levels agree well with our results for both cut-offs and the two $Z_c(3900)$ state interpretations examined in this work. The higher energy levels are the relevant ones, and, as already mentioned, our results are significantly shifted to lower energies with respect to $E^{(1)}_{D^*\bar{D}}$ for the resonant sce-

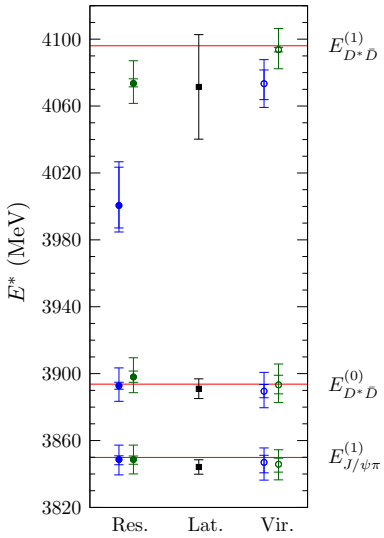

Fig. 3 Comparison of the energy levels of Ref. [48], shown with *black squares*, with our results for $L \simeq 2$ fm. Full (*empty*) *circles* stand for the energy levels obtained in the resonance (virtual state) scenario for the $Z_c(3900)$ state. On the other hand, the energy levels for the $\Lambda_2 = 1$ GeV (0.5 GeV) case are shown by *blue* (*green*) *circles*. The energy levels calculated in this work are displayed with two types of *error bars*: the *smaller ones* have been obtained considering only the errors of the parameters entering in the T-matrix (Table 1), whereas the *larger ones* additionally take into account the errors of the lattice parameters (Table 2)

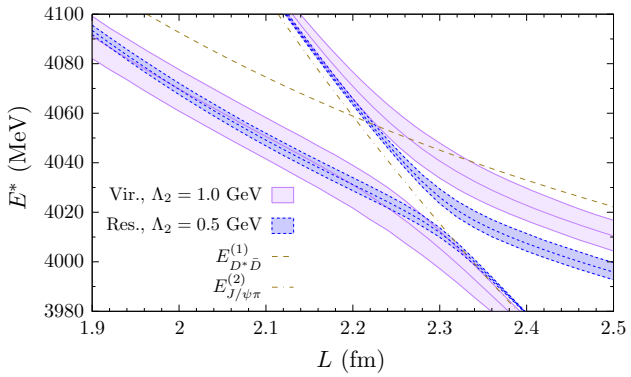

Fig. 4 Comparison of the relevant energy level for the $\Lambda_2 = 1$ GeV virtual state (*solid purple lines*) and the $\Lambda_2 = 0.5$ GeV resonance scenarios (*dashed blue lines*) around $L \simeq 2$ fm. The *green dashed* and *dashed-dotted lines* represent $E^{(1)}_{D^*\bar{D}}$ and $E^{(2)}_{J/\psi\pi}$ non-interacting energies, respectively

nario, while this shift is much smaller for the virtual state one. In general, the lattice results are in very good agreement with the virtual state scenario level for both $\Lambda_2 = 0.5$ GeV and $\Lambda_2 = 1$ GeV cases, whereas in the resonance scenario the agreement is also very good for $\Lambda_2 = 0.5$ GeV, and it is not so good for $\Lambda_2 = 1$ GeV. However, in the latter case, we find $E_{\rm th} = 4000^{+24}_{-13}$ MeV, while the lattice energy is $E_{\rm lat} = 4070 \pm 30$ MeV [48], and hence this non-compatibility is small, the difference being $E_{\rm lat} - E_{\rm th} = 70 \pm 40$ MeV. The comparison of our results with those of Ref. [48] supports the conclusions given in the latter work: from the energy levels found in that LQCD simulation one cannot deduce the existence of a resonance (a truly physical state, instead of a virtual state), namely $Z_c(3900)$. But also from this comparison, putting this conclusion the other way around, one cannot discard its existence either.

Finally, as can be seen in Fig. 3, a comparison of the relevant energy level obtained in the resonance scenario for $\Lambda_2 = 0.5$ GeV (green filled circle) with that obtained in the virtual scenario for $\Lambda_2 = 1$ GeV (blue empty circle) shows that, within theoretical uncertainties (the smallest error bars), the two cases are indistinguishable. This fact can already be seen by comparing the left panel of Fig. 2 and the right panel of Fig. 1 around $L \simeq 2$ fm. These energy levels are shown together in Fig. 4. It can be seen that, although these two scenarios cannot be distinguished at $L \simeq 2$ fm (the volume used in Ref. [48]), they lead to appreciably different energies already at $L \simeq 2.5$ fm. This means that one cannot elucidate the nature of this intriguing $Z_c(3900)$ state with LQCD simulations performed in a single volume. Rather, it would be useful to perform simulations at different values of the box size, to properly study the volume dependence of the energy levels. Of course, as discussed in Ref. [48], this would bring about a technical problem—the appearance of more $J/\psi\pi$ free energy levels in the energy region of interest,[6] as can be seen in Fig. 4 ($E^{(2)}_{J/\psi\pi}$). Notwithstanding these difficulties, our work should stimulate this kind of studies.

It must also be stated that there are certainly other ways to perform LQCD simulations to gain further insight on the nature of $Z_c(3900)$ that do not require the use of several volumes. One can perform, for example, simulations in a single volume but with the two-meson systems moving with several non-zero momentum [65–68] (examples of such type of simulations can be found e.g. in Refs. [60,61,69]). Results of such approaches could not be directly compared, however, with our results presented in Sect. 3, where we have focused on the volume dependence of the discrete spectrum obtained in LQCD calculations. Although it is beyond the scope of this work, we would like to mention that it is also possible to make predictions from unitary effective field theories for such simulations [58].

4 Summary

With the aim of shedding light into the nature of the $Z_c(3900)$ state, we have implemented the $J/\psi\pi$, $D^*\bar{D}$ coupled-channel T-matrix of Ref. [35] in a finite volume, and we have compared our predictions with the results obtained in

[6] It should be noted that recent analysis of LQCD simulations (e.g. Refs. [60,61]) are able to obtain detailed spectra involving a large number of energy levels, overcoming this difficulty.

the LQCD simulation of Ref. [48]. The model of Ref. [35] provides a similar good description of the experimental information concerning the $Z_c(3900)$ structure in two different scenarios. In the first one, the $Z_c(3900)$ structure is due to a resonance originating from the $D^*\bar{D}$ interaction, while in the second one it is produced by the existence of a virtual state. We have studied the dependence of the energy levels on the size of the finite box for both scenarios. For the volume used in Ref. [48], our results compare well with the energy levels obtained in the LQCD simulation of Ref. [48]. However, the agreement is similar in both scenarios (resonant and virtual) and hence it is not possible to privilege one over the other. Therefore and in order to clarify the nature of the $Z_c(3900)$ state, we suggest performing further LQCD simulations at different volumes to study the volume dependence of the energy levels.

Acknowledgments We would like to thank S. Prelovsek for reading the manuscript and for useful discussions. MA acknowledges financial support from the "Juan de la Cierva" program (27-13-463B-731) from the Spanish MINECO. This work is supported in part by the Spanish MINECO and European FEDER funds under the contracts FIS2014-51948-C2-1-P, FIS2014-57026-REDT and SEV-2014-0398, and by Generalitat Valenciana under contract PROMETEOII/2014/0068.

References

1. S.K. Choi et al. [Belle Collaboration], Phys. Rev. Lett. **91**, 262001 (2003)
2. S.L. Olsen, Front. Phys. **10**, 101401 (2015)
3. H.X. Chen, W. Chen, X. Liu, S.L. Zhu. arXiv:1601.02092 [hep-ph]
4. A. Hosaka, T. Iijima, K. Miyabayashi, Y. Sakai, S. Yasui. arXiv:1603.09229 [hep-ph]
5. S. Godfrey, N. Isgur, Phys. Rev. D **32**, 189 (1985)
6. M. Ablikim et al. [BESIII Collaboration], Phys. Rev. Lett. **110**, 252001 (2013)
7. Z.Q. Liu et al. [Belle Collaboration], Phys. Rev. Lett. **110**, 252002 (2013)
8. T. Xiao, S. Dobbs, A. Tomaradze, K.K. Seth, Phys. Lett. B **727**, 366 (2013)
9. M. Ablikim et al. [BESIII Collaboration], Phys. Rev. Lett. **112**, 022001 (2014)
10. M. Ablikim et al. [BESIII Collaboration], Phys. Rev. D **92**, 092006 (2015)
11. M. Ablikim et al. [BESIII Collaboration], Phys. Rev. Lett. **115**, 112003 (2015)
12. M.B. Voloshin, Phys. Rev. D **87**, 091501 (2013)
13. Q. Wang, C. Hanhart, Q. Zhao, Phys. Rev. Lett. **111**, 132003 (2013)
14. F.K. Guo, C. Hidalgo-Duque, J. Nieves, M.P. Valderrama, Phys. Rev. D **88**, 054007 (2013)
15. E. Wilbring, H.-W. Hammer, U.-G. Meißner, Phys. Lett. B **726**, 326 (2013)
16. Y. Dong, A. Faessler, T. Gutsche, V.E. Lyubovitskij, Phys. Rev. D **88**, 014030 (2013)
17. J.R. Zhang, Phys. Rev. D **87**, 116004 (2013)
18. H.W. Ke, Z.T. Wei, X.Q. Li, Eur. Phys. J. C **73**, 2561 (2013)
19. F. Aceti et al., Phys. Rev. D **90**, 016003 (2014)
20. J. He, Phys. Rev. D **92**, 034004 (2015)
21. E. Braaten, Phys. Rev. Lett. **111**, 162003 (2013)
22. J.M. Dias, F.S. Navarra, M. Nielsen, C.M. Zanetti, Phys. Rev. D **88**, 016004 (2013)
23. Z.G. Wang, T. Huang, Phys. Rev. D **89**, 054019 (2014)
24. C.F. Qiao, L. Tang, Eur. Phys. J. C **74**, 3122 (2014)
25. C. Deng, J. Ping, F. Wang, Phys. Rev. D **90**, 054009 (2014)
26. A. Esposito, A.L. Guerrieri, F. Piccinini, A. Pilloni, A.D. Polosa, Int. J. Mod. Phys. A **30**, 1530002 (2015)
27. L. Maiani, F. Piccinini, A.D. Polosa, V. Riquer, Phys. Rev. D **89**, 114010 (2014)
28. Z.Y. Zhou, Z. Xiao, Phys. Rev. D **92**, 094024 (2015)
29. D.Y. Chen, X. Liu, T. Matsuki, Phys. Rev. D **88**, 036008 (2013)
30. E.S. Swanson, Phys. Rev. D **91**, 034009 (2015)
31. A.P. Szczepaniak, Phys. Lett. B **747**, 410 (2015)
32. S. Coito. arXiv:1602.07821 [hep-ph]
33. F.K. Guo, C. Hanhart, Q. Wang, Q. Zhao, Phys. Rev. D **91**, 051504 (2015)
34. M. Cleven, F.K. Guo, C. Hanhart, Q. Wang, Q. Zhao, Phys. Rev. D **92**, 014005 (2015)
35. M. Albaladejo, F.K. Guo, C. Hidalgo-Duque, J. Nieves, Phys. Lett. B **755**, 337 (2016)
36. Z. Fodor, C. Hoelbling, Rev. Mod. Phys. **84**, 449 (2012)
37. J.J. Dudek, R.G. Edwards, N. Mathur, D.G. Richards, Phys. Rev. D **77**, 034501 (2008)
38. G.S. Bali, S. Collins, C. Ehmann, Phys. Rev. D **84**, 094506 (2011)
39. L. Liu et al. [Hadron Spectrum Collaboration], JHEP **1207**, 126 (2012)
40. C.B. Lang, L. Leskovec, D. Mohler, S. Prelovsek, JHEP **1509**, 089 (2015)
41. M. Luscher, Commun. Math. Phys. **105**, 153 (1986)
42. M. Luscher, Nucl. Phys. B **354**, 531 (1991)
43. C. Liu, X. Feng, S. He, Int. J. Mod. Phys. A **21**, 847 (2006)
44. M. Lage, U.G. Meissner, A. Rusetsky, Phys. Lett. B **681**, 439 (2009)
45. V. Bernard, M. Lage, U.-G. Meissner, A. Rusetsky, JHEP **1101**, 019 (2011)
46. M. Doring, U.G. Meissner, E. Oset, A. Rusetsky, Eur. Phys. J. A **47**, 139 (2011)
47. S. Prelovsek, L. Leskovec, Phys. Lett. B **727**, 172 (2013)
48. S. Prelovsek, C.B. Lang, L. Leskovec, D. Mohler, Phys. Rev. D **91**, 014504 (2015)
49. Y. Chen et al., Phys. Rev. D **89**, 094506 (2014)
50. L. Liu et al., PoS LATTICE **2014**, 117 (2014)
51. S.H. Lee et al. [Fermilab Lattice and MILC Collaborations]. arXiv:1411.1389 [hep-lat]
52. Y. Ikeda et al. arXiv:1602.03465 [hep-lat]
53. M. Albaladejo, C. Hidalgo-Duque, J. Nieves, E. Oset, Phys. Rev. D **88**, 014510 (2013)
54. E.J. Garzon, R. Molina, A. Hosaka, E. Oset, Phys. Rev. D **89**, 014504 (2014)
55. J. Nieves, M.P. Valderrama, Phys. Rev. D **86**, 056004 (2012)
56. C. Hidalgo-Duque, J. Nieves, M.P. Valderrama, Phys. Rev. D **87**, 076006 (2013)
57. M. Albaladejo, F.-K. Guo, C. Hidalgo-Duque, J. Nieves, M.P. Valderrama, Eur. Phys. J. C **75**, 547 (2015)
58. M. Doring, U.G. Meissner, E. Oset, A. Rusetsky, Eur. Phys. J. A **48**, 114 (2012)
59. C.B. Lang, L. Leskovec, D. Mohler, S. Prelovsek, R.M. Woloshyn, Phys. Rev. D **90**, 034510 (2014)
60. D.J. Wilson, J.J. Dudek, R.G. Edwards, C.E. Thomas, Phys. Rev. D **91**, 054008 (2015)

61. J.J. Dudek et al. [Hadron Spectrum Collaboration], Phys. Rev. D **93**, 094506 (2016)
62. J. Nebreda, J.R. Pelaez, Phys. Rev. D **81**, 054035 (2010)
63. C. Hanhart, J.R. Pelaez, G. Rios, Phys. Rev. Lett. **100**, 152001 (2008)
64. M. Albaladejo, J.A. Oller, Phys. Rev. D **86**, 034003 (2012)
65. K. Rummukainen, S.A. Gottlieb, Nucl. Phys. B **450**, 397 (1995)
66. C.H. Kim, C.T. Sachrajda, S.R. Sharpe, Nucl. Phys. B **727**, 218 (2005)
67. Z. Fu, Phys. Rev. D **85**, 014506 (2012)
68. L. Leskovec, S. Prelovsek, Phys. Rev. D **85**, 114507 (2012)
69. S. Prelovsek, L. Leskovec, C.B. Lang, D. Mohler, Phys. Rev. D **88**, 054508 (2013)